

Phosphorus emitter engineering by plasma-immersion ion implantation for c-Si solar cells

Thomas Michel, Jerome Le Perchec, Adeline Lanterne, Rémi Monna, Frank Torregrosa, Laurent Roux, Mireille Commandre

▶ **To cite this version:**

Thomas Michel, Jerome Le Perchec, Adeline Lanterne, Rémi Monna, Frank Torregrosa, et al.. Phosphorus emitter engineering by plasma-immersion ion implantation for c-Si solar cells. Solar Energy Materials and Solar Cells, 2015, 133, pp.194-200. 10.1016/j.solmat.2014.11.014 . cea-02570721

HAL Id: cea-02570721
https://cea.hal.science/cea-02570721

Submitted on 12 May 2020

HAL is a multi-disciplinary open access archive for the deposit and dissemination of scientific research documents, whether they are published or not. The documents may come from teaching and research institutions in France or abroad, or from public or private research centers.

L'archive ouverte pluridisciplinaire **HAL**, est destinée au dépôt et à la diffusion de documents scientifiques de niveau recherche, publiés ou non, émanant des établissements d'enseignement et de recherche français ou étrangers, des laboratoires publics ou privés.

Solar Energy Materials & Solar Cells 133 (2015) 194–200

Contents lists available at ScienceDirect

Solar Energy Materials & Solar Cells

journal homepage: www.elsevier.com/locate/solmat

Phosphorus emitter engineering by plasma-immersion ion implantation for c-Si solar cells

Thomas Michel [a,b,*], Jérôme Le Perchec [c], Adeline Lanterne [c], Rémi Monna [c], Frank Torregrosa [a], Laurent Roux [a], Mireille Commandré [b]

[a] IBS, Rue Gaston Imbert Prolongée, Z.I. Rousset-Peynier, 13790 Peynier, France
[b] Aix-Marseille University, Ecole Centrale Marseille, CNRS, Fresnel Institute, Avenue Escadrille Normandie-Niemen, 13397 Marseille Cedex, France
[c] CEA, LITEN, INES, 50 Avenue du Lac Léman, 73375 Le Bourget-du-Lac, France

ARTICLE INFO

Article history:
Received 24 June 2014
Received in revised form
16 October 2014
Accepted 4 November 2014
Available online 25 November 2014

Keywords:
Ion implantation
Plasma-immersion
Crystalline silicon
Solar cell
Photovoltaics

ABSTRACT

Ion Beam Services (IBS) has developed processes dedicated to silicon-based solar cell manufacturing using a plasma-immersion ion implantation equipment. It enables the realization of various doping profiles for phosphorus-doped emitters which fit the requirements of high-efficiency solar cells. PH_3 plasma-implanted emitters are chemically, physically and electrically characterized to demonstrate their excellent quality. Those emitters are then integrated into a low cost p-type monocrystalline silicon solar cell manufacturing line from the National Solar Energy Institute (INES) in order to be compared with usual $POCl_3$ diffusion. Starting from a basic process flow with blanket emitter and conventional full-area aluminum back-surface field, plasma-immersion implanted emitters enable to raise conversion efficiencies above 19.1%. Thanks to an optimized double layer anti-reflective coating, a 19.4% champion cell has been achieved. Depending on different plasma process parameters, lightly doped emitters are then engineered aiming to study doping modulation using a dedicated laser.

© 2014 Elsevier B.V. All rights reserved.

1. Introduction

Over the past few years, high conversion efficiencies above 19% have been achieved on p-type 156 mm c-Si substrates with beamline implanters dedicated to PV manufacturers [1,2]. Compared to diffusion-based doping processes, ion implantation offers a better control of the implanted dose and profile, while ensuring great uniformity and reproducibility [1]. However, the industrial integration of such a technology is rather slowed down by high implementation and running costs, since it still requires a thermal annealing step for defects healing and electrical activation of dopants [3]. Furthermore, throughputs as high as 3600 cells/h are required to fulfill the expectations of the roadmaps from the photovoltaic industry for solar cell manufacturing [4]. Plasma immersion ion implantation (PIII) reactors promise higher throughput, less investment costs and lower cost of ownership. Unlike beamline implantation, doping duration is not dependent on the implanted surface and it also offers the capability of a conformal doping, which is of particular interest for advanced textured surfaces [5] and cell architectures. IBS has developed, over the last 10 years, its own plasma doping tool. PULSION®'s key feature is a proprietary remote radio frequency plasma source that enables high density plasmas with a low chamber pressure. It results in a wide process space and a specific chamber design that optimizes the doping uniformity (cf. Fig. 1) [6].

Although the first publication from IBS about PIII for crystalline silicon solar cells dates back to 2004 [7], only few papers have since been published about emitter implantation through plasma immersion [8]. Whereas IBS and INES demonstrated the strong relevance of PIII for high efficiency silicon solar cells [9], this paper studies the ability and flexibility of this immersion plasma implanter to perform emitter doping for high efficiency crystalline silicon solar cells. The influence of the emitter doping profile is observed through modeling and characterizations. Optimized emitters are then implemented within a low cost solar cell manufacturing process flow which enables a comparison with usual $POCl_3$ diffused emitters. We then go ahead in the doping engineering by addressing the issue of emitter differential doping based on PIII.

2. Emitter modeling and simulation

In this part we are focused on modeling emitters and solar cells using PC1D, a software which enables modeling semiconductor

* Corresponding author at: IBS, Rue Gaston Imbert Prolongée, Z.I. Rousset-Peynier, 13790 Peynier, France. Tel.: +33 442 538 923.
E-mail address: thomas.michel@ion-beam-services.fr (T. Michel).

http://dx.doi.org/10.1016/j.solmat.2014.11.014
0927-0248/© 2014 Elsevier B.V. All rights reserved.

devices and simulating their electrical behavior [10,11]. The aim of this study is to get a clear understanding of the influence of the emitter doping profile on the solar cell performances.

As an initial approach, the implanted homogeneous emitter has been modeled with complementary error functions even if we will see that the distribution of phosphorus diffused into silicon has a "kink-and-tail" shape [12]. In the complementary error function, depth and level of emitter doping are adjusted by the junction depth (X_J [nm]) and the surface concentration (C_S [at/cm^3]). Our calculation takes notably account of the impact of the dopant surface concentration on the front surface recombination velocity (*FSRV* [cm/s]) as observed by Cuevas through the linear approximation: $FSRV = 10^{-16}\ \mathrm{cm^4 s^{-1}} \times C_S$ (if $C_S \geq 10^{18}$ at/cm^3) [13]. In the same way, our calculation takes into account the degradation of the fill factor (*FF*) caused by increasing emitter sheet resistance. An empirical approximation is implemented within the model to make a link between the contact resistance (R_C in Ωcm^2) and the sheet resistance (R_{sq} in Ω/sq) of the emitter for dopant surface concentrations between 10^{20} and 10^{21} at/cm^3: $R_C = -0.0275 + 0.000445\ \mathrm{cm^2} \times R_{sq}$ (if $R_{sq} > 64\ \Omega$/sq), otherwise $R_C = 0.001\ \Omega\ \mathrm{cm^2}$ [14].

Fig. 2 shows the variation of respectively the emitter sheet resistance and the conversion efficiency (*CE*) according to C_S and X_J. Through the comparison between the two diagrams, we see that the conversion efficiency is maximum for emitter sheet resistances around 60 Ω/sq. Moreover, improvement of the metallization paste will decrease the contact resistance. Thus that should enable engineering of less doped (around 100 Ω/sq) and shallower emitters which enhance the blue response of the devices. In this way, pairing of implantation and thermal annealing adds some process flexibility to design tailored fit emitters.

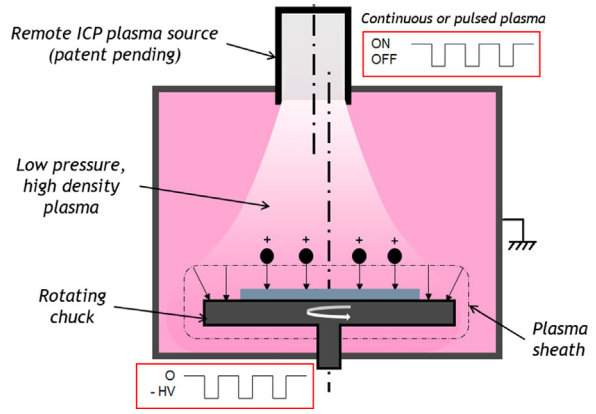


Fig. 1. Functional diagram of PULSION® ion implanter. Key features are a remote plasma source and a biased substrate being immersed in the plasma.

3. Description of experiments

This paper highlights the process development of plasma-immersion ion implantation for the fabrication of phosphorus homogeneous emitters. All the implantation experiments have been performed with a high productivity tool designed for the semiconductor industry. Phosphine (PH_3) has been chosen as the gas precursor required to create the phosphorus based plasma. Initially, Secondary Ion Mass Spectrometry (SIMS) analyses were performed on polished silicon wafers to understand the behavior of phosphorus and hydrogen in silicon before and after thermal annealing. Healing the defects generated by the implantation is a key target to fulfill during annealing. Thus, Transmission Electron Microscopy (TEM) has been carried out before and after oxidizing annealing to confirm the integrity of the silicon bulk crystal.

PULSION® implantation of emitters has then been embedded in an industrial low cost process flow of monocrystalline silicon solar cells fabrication (cf. Fig. 3). INES supplied IBS with textured and cleaned p-type silicon wafers for homogeneous phosphorus implantation. The wafers were then shipped back for annealing and completion of the fabrication process. Note that the post-implantation thermal annealing includes the growth of a passivation oxide that inherently enhances the open-circuit voltage compared to the classical $POCl_3$-based process (with single silicon nitride passivation on the front side). INES finally performed lifetime measurements and electrical characterizations of the fabricated solar cells so as to compare plasma immersion implantation to their standard $POCl_3$ diffusion process with and without subsequent oxidation step, as highlighted by the diagram of the Fig. 3 below.

It is noteworthy that no additional cleaning has been performed between implantation and annealing steps. Indeed, neither the transport between INES and IBS nor the non-mass analyzed implantation expose the material to contamination which would significantly impact the effective lifetime of photo-carriers. Contamination is regularly monitored in combination of Vapor Phase Decomposition (VPD) and Inductively Coupled Plasma Mass Spectrometry (ICP-MS). Surface concentrations of metal contaminants are usually lower than 10^{10} cm^{-2} and almost never exceeds the 10^{12} cm^{-2} threshold on PH_3-implanted wafers.

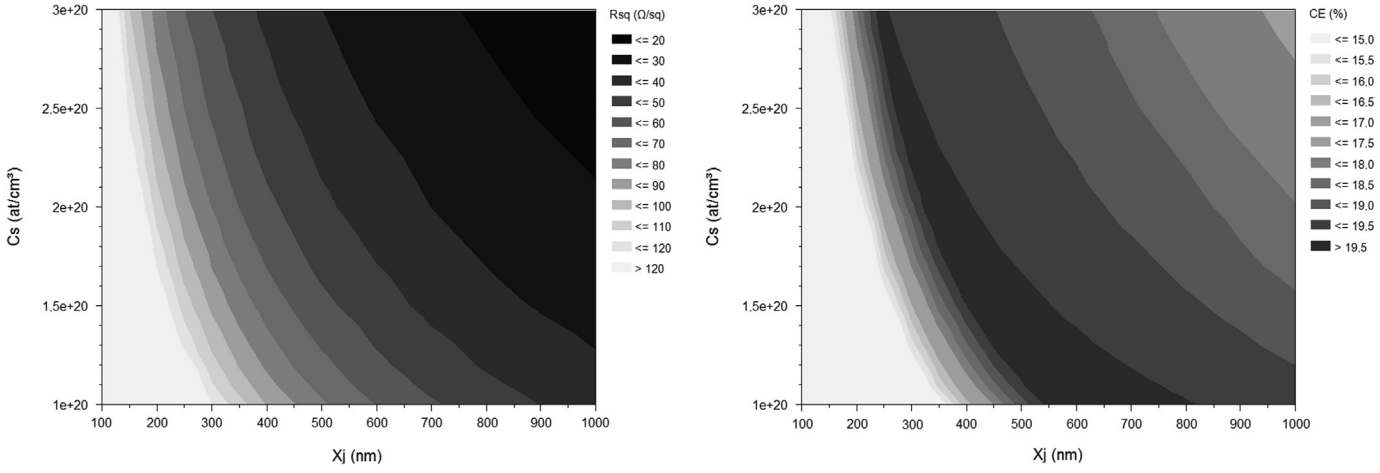


Fig. 2. Contour plot of PC1D-simulated emitter sheet resistance (R_{sq}) and conversion efficiency (*CE*), depending on junction depth (X_J) and surface concentration of dopants (C_S). Simulated efficiencies are optimal when emitter sheet resistances are around 60 Ω/sq.

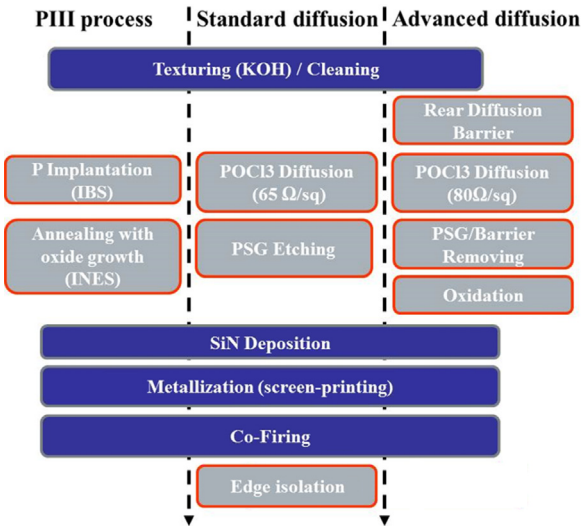


Fig. 3. Comparison of diffusion and plasma-immersion based process flows [9]. These process sequences are applied to 239 cm^2 Cz p-type solar cells. Compared to standard diffusion process flow, ion implantation adds an annealing process step whereas phosphosilicate glass (PSG) removal and edge isolation are suppressed. Note that the initial 80 Ω/sq of the advanced diffused emitter has a final sheet resistance of around 65 Ω/sq after thermal oxidation.

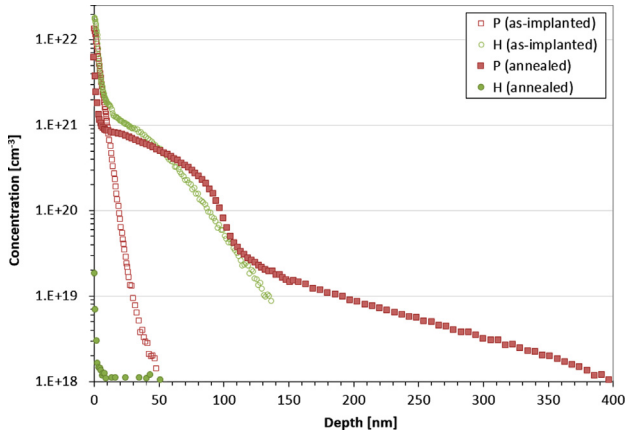


Fig. 4. Phosphorus and hydrogen SIMS profiles of a PH_3-implanted emitter. Hydrogen penetration in silicon bulk is deeper than that of phosphorus. Hydrogen almost totally outdiffuses during post-implantation annealing.

4. Phosphorus emitter implantation

First, it has to be noticed that the PH_3 gas precursor leads to the co-implantation of hydrogen through ion species such as PH_X^+, $P_2H_Y^+$ or H_Z^+. Due to the mass ratio between the two species, hydrogen is implanted deeper than phosphorus, as shown in Fig. 4. However, hydrogen is not detrimental as it almost completely outdiffuses during annealing. After furnace annealing, phosphorus SIMS profile shows a "kink-and-tail" shape for the distribution of the dopants within the silicon bulk in accordance with the vacancy-percolation model suggested by Mathiot and Pfister [12].

Left picture on Fig. 5 shows SIMS profiles of as-implanted phosphorus. Here two implantation parameters and their impact on the as-implanted phosphorus distribution have been studied: the bias voltage (E [kV]) applied to the substrate and the setpoint dose (D [at/cm^2]) which refers to the total dose of implanted ion species as measured by the equipment. Varying the bias voltage impacts the doping depth whereas the dopant surface concentration remains almost invariant. In the same way, a variation of the setpoint dose impacts the surface concentration and has almost no effect on the phosphorus implant depth.

Besides, the picture on the right (Fig. 5) demonstrates that the bias voltage – within the range of study and the given thermal budget—has no influence on the distribution of phosphorus after diffusion in the silicon bulk which is driven by the dopant surface concentration. Indeed, the high surface concentration of phosphorus acts as a tank for its diffusion into the bulk during the annealing. This diffusion mechanism may seem like a loss of freedom for emitter engineering, but it also offers the flexibility of adjusting the bias voltage as desired to fit with an optimum operating range of the implanter in terms of cost and/or throughput. Ultimately, this observation should lead to the conclusion that the bias voltage—within this range of study—has no impact on critical solar cell parameters such as emitter saturation current (J_{0e}), open-circuit voltage (V_{OC}) or fill factor.

TEM analyses have been conducted to confirm the integrity of the silicon bulk after annealing. Indeed, the post-implant annealing not only aims to the dopants electrical activation, but also enables the healing of the defects caused by the ion implantation process. Fig. 6 presents TEM images on which we can clearly see about 20 nm of amorphized silicon bulk due to the ion bombardment. After post-implantation annealing, we see the presence of the thin silicon oxide grown during the thermal treatment.

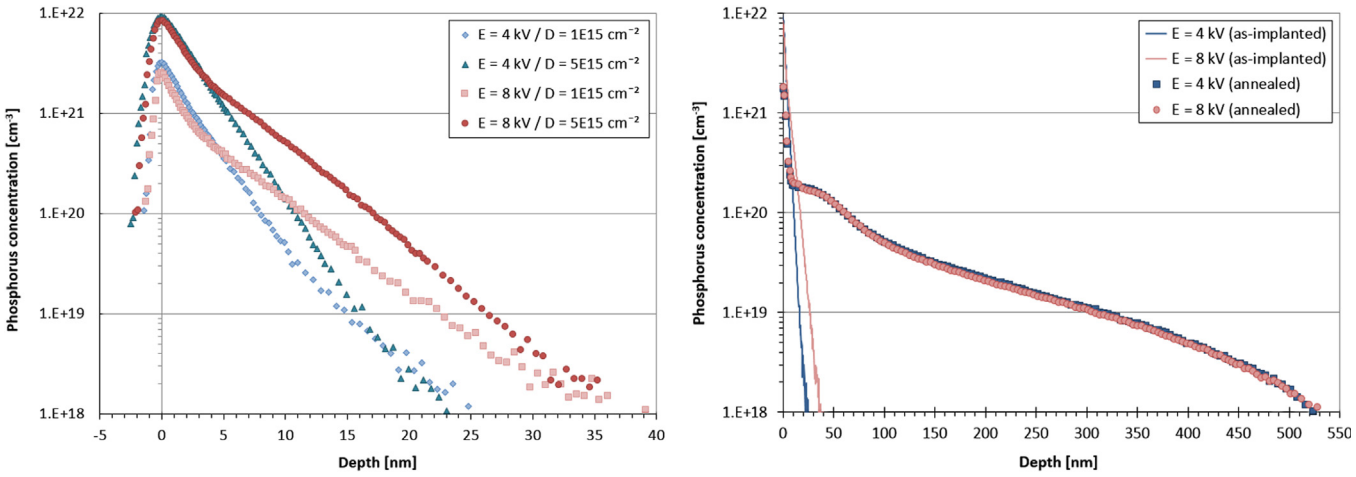


Fig. 5. Phosphorus SIMS profiles before and after annealing for different process parameters. The picture on the left shows as-implanted profiles for various bias voltages (E) and setpoint doses (D), whereas the picture on the right shows the impact of bias voltage on the doping profile after annealing. The x-axis origin indicates the interface between the bulk silicon and the surface native oxide.

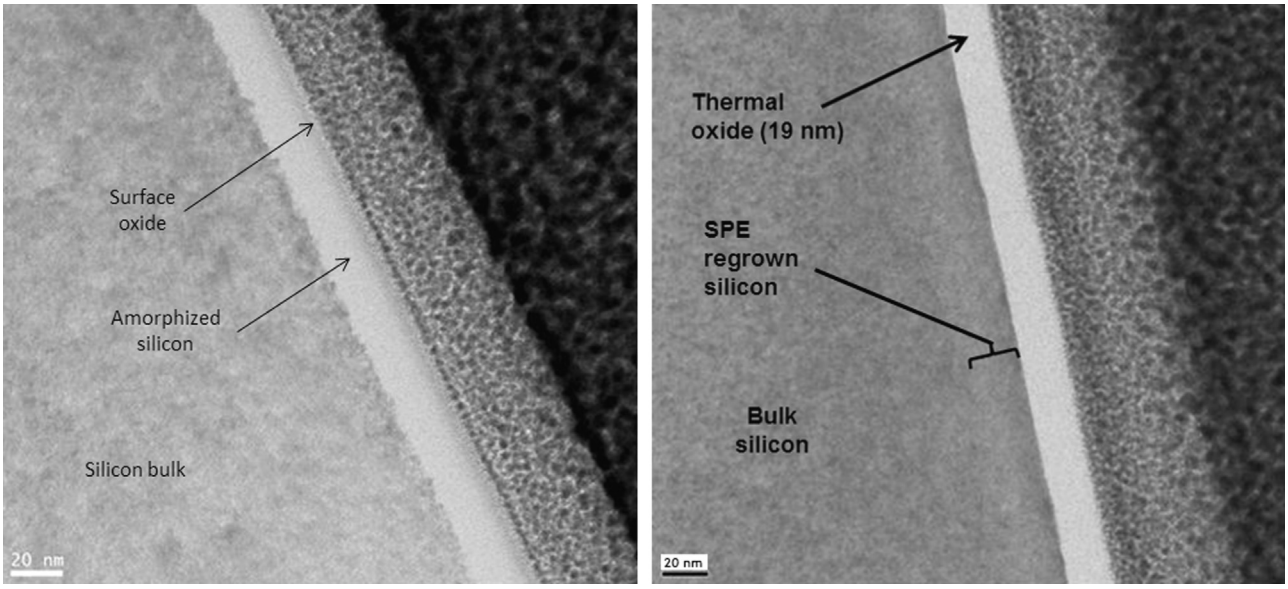


Fig. 6. TEM images of a monocrystalline silicon wafer implanted with PH_3 before and after annealing. The picture on the left shows an as-implanted sample with an amorphized silicon layer (about 20 nm thick) near the surface due to the ion bombardment. After annealing (on the right), the bulk silicon has been regrown and a thin passivating oxide (less than 20 nm) lays on top of the surface.

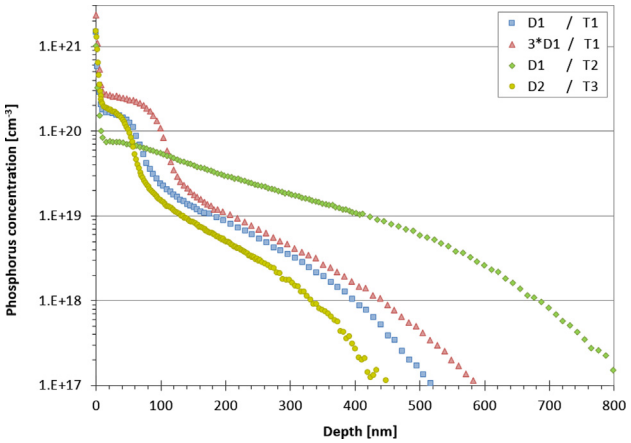


Fig. 7. Phosphorus SIMS profiles of PH_3-implanted emitters with three setpoint doses of dopants ($D_2 < D_1 < 3{*}D_1$) have been implanted. These polished samples have then been annealed at various temperatures ($T_1 < 900$ °C, $T_2 = T_1 + 100$ °C, $T_3 \approx T_1$).

Moreover a slight contrast can be observed in the bulk near the interface with the oxide: this area gives evidence of a solid-phase epitaxial recrystallization of the silicon which was amorphized by the ion bombardment. Another high resolution picture of the same wafer (not presented here) displays the atomic arrangement of the recrystallized lay and shows a clearly defined interface between the silicon and its oxide.

5. Solar cell fabrication and characterization

Here different PH_3 dopings have been performed and characterized after annealing in order to underline the impact of the phosphorus distribution on the emitter electrical performance. Four setpoint doses ranging between 10^{15} and 10^{16} at/cm^2 (D_1, $2{*}D_1$, $3{*}D_1$, $D_2 < D_1$) and three anneal temperatures ($T_1 < 900$ °C, $T_2 = T_1 + 100$ °C, $T_3 \approx T_1$) have been studied. Lifetime measurement was achieved on implanted then passivated bifacial wafers. Fig. 7 shows phosphorus SIMS profiles for several implantation and anneal conditions, whereas Table 1 recaps results of the related electrical characterizations.

Table 1
Electrical characterizations of PH_3-implanted emitters. Emitter sheet resistance (R_{sq}), implied open-circuit voltage (iV_{OC}) and emitter saturation current (J_{0e}) have been measured on polished samples, for various combinations of setpoint doses of dopants (D) and anneal temperatures (T).

Setpoint dose	Anneal temperature	Average R_{sq} on 156PSQ [Ω/sq]	iV_{OC} (after firing) [mV]	J_{0e} (after firing) [fA/cm²]
D_1	T_1	53	641	155
$2{*}D_1$	T_1	49	642	231
$3{*}D_1$	T_1	38	635	299
D_1	$T_2 = T_1 + 100$ °C	44	597	#N/A
D_2	$T_3 \approx T_1$	68	646	134

By minimizing phosphorus concentration near the surface, these doping profiles avoid electrically inactive dopants which are highly detrimental to emitter quality. In accordance with the PC1D simulations, we observe on Table 1 that higher is the setpoint dose, higher is the emitter saturation current (because of increasing Auger recombination) and thus lower is the implied open-circuit voltage (iV_{OC}).

Being annealed at high temperature, the optimized emitter (D_1, T_2) presents improved J_{0e} and iV_{OC} before firing thanks to a lower surface concentration of dopants. However, we observe a deteriorated iV_{OC} after simulating the firing process. A Light Beam Induced Current (LBIC) lifetime measurement emphasized swirl crystal defects which could have been formed during the high temperature annealing.

Table 2 compiles results from illuminated (AM1.5) *I–V* measurement of cells with those PH_3-implanted emitters. Thanks to a lower concentration of dopants, cells with emitter (D_1, T_1) show higher short-circuit current (J_{SC}) and V_{OC} than those with emitter ($3{*}D_1$, T_1) in accordance with our PC1D simulations. However these cells are less efficient because of a lower fill factor. That's why setpoint dose and anneal temperature have been optimized (D_2, T_3) to enhance both J_{SC} and V_{OC}, while the metallization step has also been improved to avoid the *FF* deterioration caused by a lower emitter doping level. A conversion efficiency of 19.15% has been obtained with emitter (D_2, T_3) and has been independently

Table 2
Electrical characterizations of solar cells with plasma-implanted emitters (with same metallization scheme). Cell electrical parameters have been obtained under an AM1.5 illumination (1 sun).

Setpoint dose	Anneal temperature	Average *Rsq* [Ω/sq]	Average J_{SC} [mA/cm²]	Average V_{OC} [mV]	Average *FF* [%]	Average *CE* [%]
$POCl_3$ diffusion without oxidation	#N/A	65	36.9	635	79.9	18.7
$POCl_3$ diffusion with oxidation	#N/A	65	37.1	644	80.1	19.15
D_1	T_1	53	37.2	637.6	78.0	18.5
$3*D_1$	T_1	38	36.3	634.3	80.9	18.7
D_2	$T_3 \approx T_1$	67	37.5	645.4	79.1	19.14

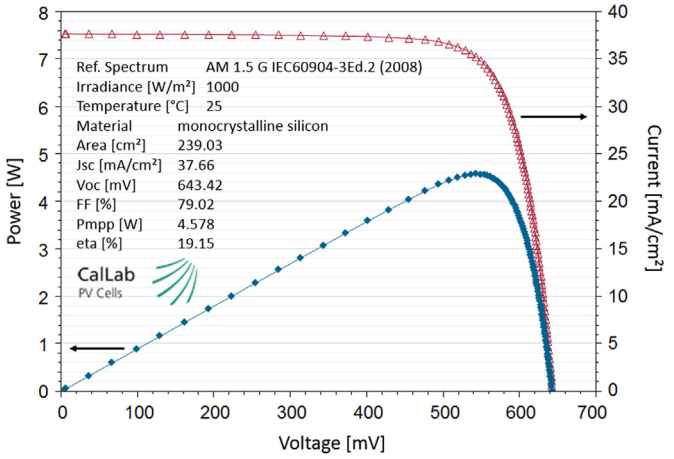


Fig. 8. *I–V* curves and electrical results for a 239 cm² textured c-Si wafer with emitter (D_2, T_3) following the PIII process flow on Fig. 3. These results have been certified by the Fraunhofer ISE CalLab.

confirmed by the Fraunhofer ISE CalLab (see Fig. 8). We thus got a gain of more than 0.4% absolute compared to $POCl_3$-based reference cells from INES. Finally, by resorting to an optimized nitride double layer anti-reflective coating, we obtained a 19.4% champion cell, and an average above 19.3% over 7 cells with almost no dispersion.

In order to accurately highlight the benefits of ion implanted emitters, PIII process sequence is also compared to lighter $POCl_3$ diffusion (80 Ω/sq recipe, see Fig. 3) followed by oxidation that significantly enhances the n-type emitter quality. Average conversion efficiencies of 19.15% have been achieved with 11 cells with a 19.28% champion cell.

Despite similar performance, we estimate that emitter engineering by ion implantation could bring an efficiency absolute gain up to 0.2% by comparison to $POCl_3$ diffusion with oxidation. However, the main advantage of PIII sequence certainly is that it requires two fewer process steps than advanced diffusion with oxidation.

6. Lightly doped emitters

There are at least two ways to continuously control the sheet resistance of implanted n-type emitters: the implantation dose and the activation annealing. Classically, the sheet resistance decreases when the dose and/or the annealing temperature increases. However, unlike beamline implanters, there is no discrimination between different ionic species ($P_XH_Y^+, H_Z^+$) in the plasma-immersion chamber. Thus, the phosphorous dose which is effectively implanted also depends on plasma and process conditions such as the chamber pressure (*P*) and the radio frequency power (*RF*) related to the induction plasma technology. Indeed, varying the chamber pressure through the incoming PH_3 gas flow impacts the residence time of gas molecules within the source as well as the electron temperature of the plasma [15]. This is the point we address in this section: studying plasma/process conditions to achieve lightly doped emitters, which can be a starting point for engineering selective emitters.

Table 3
Electrical parameters and cell performances on 239 cm² textured c-Si wafers, for different process conditions. Cell electrical parameters have been obtained under an AM1.5 illumination (1 sun).

Process conditions: $RF_0 < RF_1$ and $P_1 < P_0$	RF_0/P_0	RF_0/P_1	RF_1/P_0
Sheet resistance [Ω/sq]	70.5	117.7	90.5
iV_{OC} before firing [mV]	641	656	653
iV_{OC} after firing [mV]	645	620	637
J_{0e} after firing [fA/cm²]	141	77	43
J_{SC} [mA/cm²]	37.5	36.8	37.7
V_{OC} [mV]	645.2	641.0	647.9
FF [%]	79.1	51.9	73.0
Pseudo-FF [%]	83.0	77.1	81.9
Efficiency [%]	19.14	12.25	17.90

After cleaning, textured Cz–silicon wafers of resistivity between 1 and 3 Ωcm were homogeneously implanted to realize solar cells according to the industrial process already developed by INES in previous works (see Fig. 3). Concerning the emitter implantation step, two chamber pressures ($P_1 < P_0$, ranging between 10^{-4} and 10^{-2} mbar) and r.f. powers ($RF_0 < RF_1$) have been studied while bias voltage, setpoint dose and annealing parameters were kept unchanged. Some wafers were double-side implanted and passivated after annealing so as to evaluate implied open-circuit voltages and emitter saturation currents, whereas polished wafers were also implanted for SIMS measurement of the emitter doping profile.

Table 3 provides electrical results for the different process parameters: (RF_0, P_0) which are the standard conditions, (RF_0, P_1) and (RF_1, P_0). Following the explanation reported in the previous section, we observe a variation of the emitter sheet resistance which can be related to different ion compositions of the plasma. First, increasing the r.f. power from RF_0 to RF_1 leads to a higher emitter sheet resistance. SIMS profiles in Fig. 9 show that this r.f. power increase results in a lower implanted dose of phosphorus which could be explained by a predominance of $P_1H_X^+$ ions over $P_2H_Y^+$ ions in the plasma at higher r.f. powers. On the other hand, decreasing the chamber pressure leads to a higher emitter sheet resistance. Lowering the injected gas flow increases the residence time of PH_3 molecules within the source. This results in an increased dissociation of phosphine molecules and thus in a higher proportion of hydrogen species into the plasma. That is why we observe a lower implanted dose of phosphorus regarding to a constant total ion dose.

As shown in Table 3 and despite showing good iV_{OC} after annealing, lightly doped emitters (RF_0, P_1) and (RF_1, P_0) are less robust after firing (possible sensitivity to surface depletion). As these lightly doped process conditions lead to high proportions of implanted hydrogen regarding to the total implanted dose, we might also have concerns about possible formation of voids or nanocavities after outdiffusion of large amounts of hydrogen gas

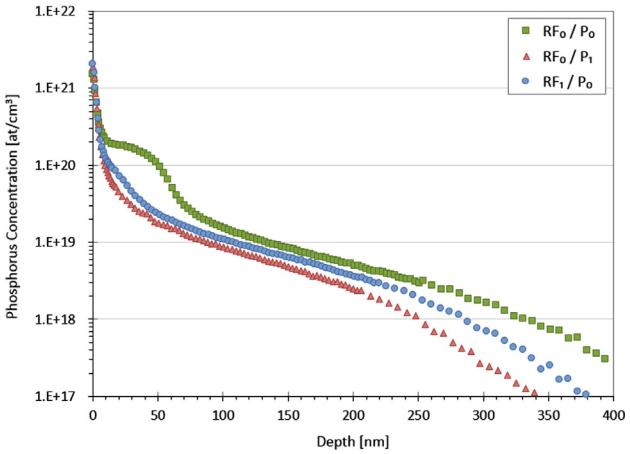


Fig. 9. Phosphorus SIMS profiles after annealing on 100 mm polished Cz–Si wafers, for different r.f. power and chamber pressure conditions ($P_1 < P_0$, $RF_0 < RF_1$). The *x*-axis origin indicates the interface between the bulk silicon and the surface oxide.

[16]. However hydrogen implantation doses that are required to form cavities are about a decade higher than those co-implanted with phosphorus in this study.

Besides these severe voltage drops after firing, the fill factors also dramatically fall due to strong series resistances and/or emitter shunting during the co-firing. This is well consistent with the SIMS profiles displayed in Fig. 9 (obtained on polished wafers with same implantation dose as textured wafers). Thus, the non-standard conditions presented here are not relevant to achieve efficient homogeneous emitters. Obviously, another way to reduce the effective doping would be to directly decrease the total implantation dose instead of changing r.f. power and pressure parameters.

7. Laser doping modulation

Although 70 Ω/sq homogeneous implanted emitters are already of high quality, it is interesting to study the possibility to make differential doping profiles to fabricate a selective emitter starting from light blanket implantations, that is to say without using shadow masks for instance by using the specific as-implanted profile of the PIII technology. In this framework, INES suggests to exploit a specific nanosecond green laser to slightly modulate the sheet resistance of the emitter after thermal annealing [17], with or without oxidation. Such a technique is an interesting and flexible alternative to selective implantation through shadow masking [1]. It has also been tested on PIII emitters by another research team but no cell results were given [18].

In the previous section, the process conditions around (RF_1, P_0) could be quite relevant to realize the initial lightly doped emitter (90 Ω/sq). Fig. 10 shows local modulation of the sheet resistance by laser control for two lightly doped n-type emitters presenting the same initial sheet resistance, with and without oxide passivation. Laser doping of a diffusion-based emitter ($POCl_3$) reference is also displayed for comparison. We note a significant decrease of the sheet resistance with increasing laser fluences. Starting from an initial 90 Ω/sq (after thermal annealing), we can obtain nearly 65 Ω/sq for PIII emitters, and less than 40 Ω/sq for the $POCl_3$ case in which the emitter still exhibits the PSG layer on top. It is worth noting that the laser flows used here are relatively low and thus do not deteriorate the surface state. We also note that the sheet resistance is lower without oxide layer, as the superficial oxidation consumes some phosphorus atoms that are not totally activated afterwards.

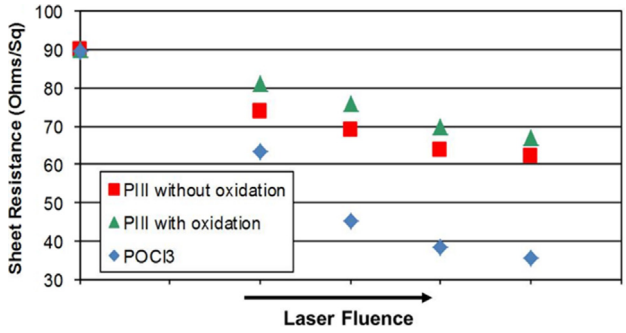


Fig. 10. Local modulation of the sheet resistance by laser control for two lightly doped n-type emitters. Laser doping of a light diffusion-based emitter ($POCl_3$) reference is also displayed for comparison.

Unlike diffusion-based processes where the phosphosilicate glass can be used as an important doping source when the laser scans the surface, there is no such doping source at the emitter surface. As a consequence, this drive-in allows minimizing the risks to shunt the light emitter through the metallizations' firing but should not be too pronounced in order to keep a sufficiently high surface concentration.

However, this significant sheet resistance decrease cannot just be explained by a drive-in mechanism. Additional dopant activation could come from phosphorus trapped inside the oxide or within the first nanometers of silicon bulk (phosphorus pile-up due to segregation at the interface Si–SiO_2 [19] as shown on Fig. 9). By this way, further experiments (SIMS profiles and contact resistance measurement) should be performed to check whether high laser fluences can lead to significant sheet resistance decreases without weakening contact resistance for future metallization.

8. Conclusion and perspectives

This work has led to the development of processes dedicated to silicon-based solar cell manufacturing using a plasma-immersion ion implantation equipment. We showed that PIII enables the realization of various doping profiles for phosphorus-doped emitters which fit the requirements for high-efficiency solar cells. Emitters thus fabricated were chemically, physically and electrically characterized to demonstrate their excellent quality. Integrated into a low cost solar cell manufacturing line from INES on monocrystalline silicon, those emitters enable to achieve conversion efficiencies up to 19.4% with a nitride double layer anti-reflective coating.

We also illustrated some non-standard conditions which give lightly doped emitters that could be used to perform selective emitters. By exploiting a drive-in mechanism, a laser scan allows a significant decrease of the local sheet resistance. This could be a practical and promising alternative to masking techniques for differential doping engineering.

Thanks to this work, the strength and potential of PIII for photovoltaic applications have been proven and this has convinced IBS to design and fabricate an equipment dedicated to solar cell manufacturing.

Acknowledgments

This research was conducted under the CIFRE process initiated by the French Ministry of Higher Education and Research. These results have been partly achieved within the PULSARCELL project supported by the French FUI.

References

[1] A. Gupta, R.J. Low, N. Bateman, D. Ramappa, H.J. Gossman, Q. Zhai, P. Sullivan, W. Skinner, C. Dubé, B. Tsefrekas, J. Mullin, High efficiency selective emitter cells using in-situ patterned ion implantation, in: Proceedings of the 25th EU PVSEC, 2010, pp. 1158–1162.

[2] A. Rohatgi, D.L. Meier, B. McPherson, Y.W. Ok, A.D. Upadhyaya, J.H. Lai, F. Zimbardi, High-throughput ion-implantation for low-cost high-efficiency silicon solar cells, Energy Proc. 15 (2012) 10–19.

[3] J.D. Plummer, M.D. Deal, P.B. Griffin, Silicon VLSI Technology: Fundamentals, Practice and Modeling, Prentice Hall, Upper Saddle River, NJ, 2000 (Implantation—Chapter 8).

[4] SEMI PV Group, International Technology Roadmap for Photovoltaic, 5th Edition, 2014, ⟨http://www.itrpv.net/Reports/Downloads/⟩ (last accessed: June 2014).

[5] T. Sarnet, T. Derrien, R. Torres, P. Delaporte, F. Torregrosa, M.J. Sher, Y.T. Lin, B. Franta, G. Deng, E. Mazur, Black silicon for photovoltaic cells: towards high-efficiency silicon solar cells, in: Proceedings of the 28th EU PVSEC, 2013, pp. 1882–1886.

[6] S.B. Felch, F. Torregrosa, H. Etienne, Y. Spiegel, L. Roux, D. Turnbaugh, PULSION® HP: Tunable, high productivity plasma doping, AIP Conf. Proc. 1321 (2010) 333–336.

[7] F. Torregrosa, C. Laviron, H. Faik, D. Barakel, F. Milesi, S. Beccaccia, Realization of ultra shallow junctions by PIII: application to solar cells, Surf. Coat. Technol. 186 (2004) 93–98.

[8] T. Janssens, N.E. Posthuma, E. van Kerschaver, K. Baert, P. Choulat, J.L. Everaert, J. Goosens, W. Vandervorst, J. Poortmans, Advanced phosphorus emitters for high efficiency si solar cells. in: Proceedings of the 34th IEEE PVSC, 2009, pp. 878–882.

[9] J. Le Perchec, A. Lanterne, T. Michel, S. Gall, R. Monna, F. Torregrosa, L. Roux, 19.3% efficiency on p-type silicon solar cells by PULSION® plasma-immersion implantation, Energy Proc. 33 (2013) 18–23.

[10] University of New South Wales, PC1D, ⟨http://www.engineering.unsw.edu.au/energy-engineering/pc1d-software-for-modelling-a-solar-cell/⟩ (last accessed: June 2014).

[11] P.A. Basore, Numerical modeling of textured silicon solar cells using PC-1D, IEEE Trans. Electron. Dev. 37 (1990) 337–343.

[12] D. Mathiot, J.C. Pfister, Dopant diffusion in silicon: a consistent view involving nonequilibrium defects, J. Appl. Phys. 55 (1984) 3518–3530.

[13] A. Cuevas, P.A. Basore, G. Giroult-Matlakowski, C. Dubois, Surface recombination velocity of highly doped n-Type silicon, J. Appl. Phys. 80 (1996) 3370–3375.

[14] D. Grote, M. Hermle, E.A. Wotke, U. Belledin, M. Hörteis, M. Spitz, M. Kasemann, S. Rein, D. Biro, W. Warta, Analyzing the effects of laterally varying emitter sheet resistance in combination with contact resistance, in: Proceedings of the 23rd EU PVSEC, 2008, pp. 278–282.

[15] A. Anders, J. Pelletier, D.M. Goebel, B.P. Wood, I.G. Brown, W. Ensinger, M. Tuszewski, Plasma Sources, in: A. Anders (Ed.), Handbook of Plasma Immersion Ion Implantation and Deposition, John Wiley and Sons, 2000, pp. 406–408.

[16] A. Kouadri Boudjelthia, G. Regula, E. Ntsoenzok, M. Canino, R. Benoit, F. Torregrosa, M. Allegrezza, Trapping of metallic impurities in multicrystalline silicon wafers, in: Proceedings of the 28th EU PVSEC, 2013, pp. 1414–1417.

[17] A. Lanterne, S. Manuel, B. Paviet-Salomon, S. Gall, A. Tauzin, Implanted selective emitter solar cell by laser thermal annealing, AIP Conf. Proc. 1496 (2012) 131–134.

[18] A. Lawerenz, K. Neckermann, G. Andrä, Plasma immersion ion implantation as an alternative to diffusion and beam-line implantation for creating phosphorus doped emitters and selective emitters, in: Proceedings of the 27th EU PVSEC, 2012, pp. 1553–1557.

[19] J.D. Plummer, M.D. Deal, P.B. Griffin, Silicon VLSI Technology: Fundamentals, Practice and Modeling, Prentice Hall, Upper Saddle River, NJ, 2000 (Diffusion—Chapter 7).